



# Thermal comfort study of urban waterfront spaces in cold regions: Waterfront skyline control based on thermal comfort objectives



Jiayang Jiang <sup>a,b</sup>, Wente Pan <sup>a,b,\*</sup>, Ruinan Zhang <sup>a,b</sup>, Yang Hong <sup>a,b</sup>, Jixian Wang <sup>a,b</sup>

<sup>a</sup> School of Architecture and Design, Harbin Institute of Technology, Harbin, 150001, China

<sup>b</sup> Key Laboratory of Cold Region Urban and Rural Human Settlement Environment Science and Technology, Ministry of Industry and Information Technology, Harbin, 150001, China

## ARTICLE INFO

### Keywords:

Outdoor thermal comfort  
Waterfront spaces  
Cold regions  
Urban form index  
Artificial neural network

## ABSTRACT

In waterfronts, thermal comfort is affected by climate and urban morphology. Existing studies on waterfront thermal comfort have mainly focused on warm and hot regions, focusing on the cooling effects of water and vegetation during the summer. The research methods are mostly questionnaire surveys and simulations, whereas the urban form and climate characteristics of cold regions are rarely considered, and the results of these studies are seldom applied to design practices. This study focused on the thermal comfort of waterfronts in cold regions. Computational Fluid Dynamics, Mean Radiant Temperature, and the Universal Thermal Climatic Index were used to examine the effects of tree–water features (winter river ice and tree defoliation) on thermal comfort in cold regions, and correlation analyses were combined to screen for relevant urban morphology factors for waterfront thermal comfort. Regression analyses were conducted to understand the influence of six factors, namely, building orientation, floor area ratio, open space ratio, building height to distance between river and building ratio, standard deviation of the first building row, and vegetation concentration, on waterfront thermal comfort. After training and comparing the four thermal comfort prediction models, a genetic algorithm combined with an artificial neural network was applied to optimize the design of the urban morphology of the six waterfront blocks. The optimization improved the waterfront thermal comfort performance by 22%, 7%, 77%, 106%, 3%, and 3%, respectively.

## 1. Introduction

The global population is expected to exceed 10 billion by the second half of this century, with 68% of the population living in urban areas [1, 2]. An urban waterfront space is an external urban space [3] containing diverse natural landscapes that relieve stress and promote positive emotions [4–8]. Performing outdoor activities in waterfront spaces can alleviate loneliness [9] and increase life expectancy [10]. In the past, designers have focused more on visual and aesthetic aspects when designing waterfront spaces [11] and less on thermal comfort, thereby reducing the efficiency of waterfront space utilization [12–14]. As people become more health-conscious, waterfront thermal comfort has received increasing attention [15].

Some scholars have explored the effects of water and vegetation on the thermal comfort of the waterfront. Tominaga et al. (2015) investigated the effect of surface evaporative cooling on the surrounding thermal environment via computational fluid dynamics (CFD)

simulation and radiative heat transfer analysis. They found that the maximum air temperature drop caused by water was approximately 2 °C [16]. Jiang et al. (2020) studied the cooling effect of waterfront green space with three typical waterfront green spaces in Shanghai [17]. Shi et al. (2020) investigated the waterfront space in Chongqing and determined the effect of air temperature reduction in green and blue spaces near the water. In addition, a decrease in the leaf area index causes the air temperature to decrease [18]. Fei et al. (2022) investigated the thermal environment under the coupling of water and greenery in Tianjin's waterfront space and evaluated the summer thermal environment of different types of microscale waters [19]. Fei et al. (2022) explored the influence of water on the microclimate of waterfront spaces using questionnaires and field measurements, and found that the intensity of the cooling effect of water was intrinsically correlated with the distance of the measured site from the center of the water [20].

Another group of scholars investigated the effects of urban form parameters on waterfront thermal comfort. Song et al. (2016) used CFD

\* Corresponding author. School of Architecture and Design, Harbin Institute of Technology, Harbin, 150001, China.

E-mail address: [panwente@hit.edu.cn](mailto:panwente@hit.edu.cn) (W. Pan).

Nomenclature	
CFD	Computational fluid dynamics
MRT	Mean radiant temperature
UTCI	Universal thermal climatic index Physiological equivalent temperature
PET	Physiological equivalent temperature
ANN	Artificial neural network
GA	Genetic algorithm
UCM	Urban canopy model
BH	Building height
BH.FR	Building height of first building row
SDBH	Standard deviation of building height
SDBH.FR	Standard deviation of first building row
FAR	Floor area ratio
BCR	Building coverage ratio
BO	Building orientation
ABPW	Angle between building and prevailing wind
OSR	Open space ratio
BVR	Building to void ratio
DRFR	Distance from river to first building row
WWDR	Width of waterfront to distance between river and building ratio
BHDR	Building height to distance between river and building ratio
WW	Width of waterfront
VCov	Vegetation coverage
VCon	Vegetation concentration
VD	Vegetation distribution

to simulate the microclimates of four representative cold waterfront districts and found that the height of frontal buildings had a greater effect on water vapor diffusion [21]. Xu et al. (2022) studied the relationship between urban form and air temperature in the waterfront area of Wuhan and analyzed the mechanisms by which urban form parameters such as building density, vegetation coverage, volume ratio, and sky view fraction affect air temperature [22]. Peng et al. (2022) performed a study on thermal comfort in urban waterfront pedestrian spaces and found that the built-up density of an area can affect air temperature oscillations [15]. Jang et al. (2022) used ENVI-met software to investigate the effects of building height restrictions, ventilation corridors, and stepped building height changes on thermal comfort in waterfront spaces in Seoul and found that building height restrictions increased the Physiological Equivalent Temperature (PET), whereas ventilation corridors provided moderate cooling in the afternoon [23].

Simulations as well as data analyses have been conducted to propose qualitative optimization design strategies or to optimize the design of specific solutions. Jiang et al. (2020) proposed strategies for improving the microclimate of waterfront green spaces, such as increasing the width and openness of green spaces and improving the connectivity of green corridors [17]. Xi et al. (2022) proposed a strategy for the layout of daylight and shade path rest facilities in cold waterfront parks [24]. Fei et al. (2022) optimized the design of riparian morphology and lawn spacing for waterfront spaces in Tianjin [20]. Wang et al. (2022) optimized the design of Hangzhou waterfront settlements based on the levels of wind channel structure, road network optimization, and three-dimensional space development intensity control [25]. Currently, there is a lack of pervasive and quantitative methods for the optimal design of waterfront spaces in the field of waterfront thermal comfort. The introduction of machine learning may change this, as a combination of machine learning and optimization-based methods can establish relationships between urban-form parameters and wide-area performance metrics to improve sustainable design [26–28]. Currently, machine-learning-based performance prediction methods have many applications in urban design. Waibel et al. (2019) investigated alternative models and Genetic Algorithms (GA) to optimize operational energy and thermal comfort [26]. Wu et al. (2021) adopted a Gaussian process regression model to calculate the relationship between design variables and discrete-location wind speeds [27]. Wang et al. (2021) developed an artificial neural network (ANN) prediction model based on performance simulations of outdoor thermal comfort and other metrics, and used it for building layouts [28]. Kabošová et al. (2022) optimized the design of urban layouts and building forms based on solar radiation, wind performance simulations, and Genetic Algorithms (GAs) [29]. Zheng et al. (2023) simulated the energy consumption and outdoor thermal comfort

in urban neighborhoods based on the urban canopy model (UCM) [30].

Some scholars have studied the effects of water and vegetation on waterfront thermal comfort, including the cooling effect of coupled water and vegetation and the relationship between the vegetation leaf area index and air temperature [18,19]. These studies were conducted primarily in hot or warm regions, focusing on the cooling effects of water and vegetation during the summer months. Compared with warm regions, ice on the water surface and seasonal leaf loss in cold regions cause changes in wind speed and surface radiation [31–33], and the impact of these particular tree water features on waterfront thermal comfort has been neglected in recent studies. Researchers have explored urban form factors and influence mechanisms affecting waterfront thermal comfort through field measurements and simulations, and the results have indicated that the floor area ratio (FAR), building height (BH), distance from the river to the first building row (DRFR), and building orientation (BO) may be correlation factors [21,22]. However, previous studies paid little attention to waterfront spaces in cold climates. The influence of urban form parameters on waterfront thermal comfort in cold climates needs to be further explored. Scholars have proposed qualitative optimal design strategies based on simulation experiments and data analysis or optimized the design of specific solutions; however, these optimization designs and strategies rely to a certain extent on the architect's personal experience and subjective judgments, and the simulation process requires considerable time and equipment resources [24,25]. In research on urban thermal comfort, fast machine learning prediction models have been established based on simulation results and combined with optimization algorithms for optimal design [28,29]. However, few scholars have applied machine learning prediction models to the study of waterfront thermal comfort. Based on the research gaps described above, the objectives of this study include:

1. In response to the lack of discussion on seasonal changes in tree water characteristics in cold regions (river ice and leaf fall in winter) in waterfront thermal comfort studies, the effect of seasonal changes in tree water characteristics on waterfront thermal comfort was investigated in this work through performance simulation.
2. To fill the gap in research on the influence of urban form factors on waterfront thermal comfort, the correlation between urban form factors and waterfront thermal comfort was explored and its influence mechanism was revealed through correlation and regression analyses.
3. To obtain a more objective, efficient, and universal design method for the thermal comfort optimization of cold waterfront blocks, this study first established an ANN-based prediction model for the thermal comfort of cold waterfront spaces and then applied and tested

the GA and ANN optimization methods to a real waterfront block to improve the waterfront thermal comfort.

## 2. Method

As shown in Fig. 1, the research methodology is divided into four parts. The first part established parametric models of 170 waterfront blocks in Harbin, Changchun, and Shenyang on the Rhino and Grasshopper platforms through case studies. In the second part, wind speed, Mean Radiant Temperature (MRT), and Universal Thermal Climatic Index (UTCI) were simulated for the waterfront blocks using Eddy3D. The simulation results were then compared to on-site measurements, and the U of each block was calculated. In the third part, the urban morphology parameters affecting the thermal comfort of waterfront spaces are analyzed using correlation analysis, the mechanism of urban morphology parameters on U is explored based on regression analysis, and corresponding design strategies are proposed. Finally, an ANN prediction model was trained using the urban morphology parameter dataset, and GA and ANN agent models were used to optimize the real waterfront blocks.

### 2.1. Case study

In this study, 170 waterfront architectural blocks from three cold cities (Harbin, Changchun, and Shenyang) were used as the case studies (Fig. 2 and SFigs.1–3) and investigated on-site. Digital models were built, and micrometeorological data such as wind speed, humidity, and air temperature of typical weather years were collected in the epw website (Table 1 and SFigs.4–6) [34]. Typical meteorological year data is provided by the epw database [35], compiled from the most typical 12 months of data extracted over the period 1995–2015 by the Sandia method, which matches long-term site-specific data with specific statistics, and is now widely used in compliance and certification modelling [36].

### 2.2. Digital model

#### 2.2.1. 3D model

As shown in Fig. 3(2), the city Rhino digital model data were obtained from Google 3D maps and contain geometrical information on building blocks, green field areas, and rivers. The waterfront space is located between the riverbank and the primary road. The space is divided into blocks and marked with serial numbers. The location of the vegetation was based on drone photos taken during field research.

To calculate the annual thermal comfort of waterfront spaces, this study referenced existing research and selected the cylindrical domain as the wind tunnel [37]. In Fig. 3 (1) and (2), after the grid-independence analysis shown in Table 2, considering the computational efficiency of the simulation, the block size was set to four. The Inner R was set to 15H, Outer R was set to 40H and the height was set to 5H. H indicates the height of the highest building in a selected block.

As shown in Fig. 4, to validate the simulation accuracy, actual micrometeorological data (air temperature, relative humidity, black globe temperature, and air velocity) were measured in April 2023, and four test points were selected in the waterfront spaces in Harbin. The air temperature, relative humidity, black globe temperature, and air velocity were measured using the instrument listed in Table 3, and the measurement period was between 9 a.m. and 2 p.m. from April 22nd to April 26th and December 15th to December 29th. MRT was calculated using the measured globe temperature, air temperature, and air velocity.

As shown in SFig.7 and SFig.8, the measured relative humidity and air temperature were compared with the data from the meteorological station. The results showed that the measured data were similar to those from the meteorological station, and the relative humidity did not change significantly depending on the distance from the river bank. In addition, the measured air velocity and MRT were compared with the

simulated data. The results show that  $R^2$ , root mean square error (RMSE), mean absolute error (MAE), and mean absolute percentage error (MAPE) of the wind speed in April were 0.85, 0.391, 0.291, and 0.064, respectively, and those of the MRT in April were 0.89, 2.673, 2.168, and 2.673, respectively. Meanwhile, the  $R^2$ , RMSE, MAE, and MAPE values of the wind speed in December were 0.85, 0.712, 0.559, and 0.09, respectively, and for the MRT in December were 0.89, 0.697, 0.51, and 0.007, respectively. This proves that the simulation results represent the actual measurements.

#### 2.2.2. Vegetation and river settings

The micrometeorological factors of cold cities have seasonal effects on vegetation and rivers in waterfront spaces. As shown in Table 4, in cold seasons, leaves have fallen from vegetation, the water surface freezes, and the terrain roughness index of the waterfront space in cold seasons was set as 0.12. In warm seasons, the vegetation is dense, the water surface maintains flow, and the terrain roughness index of the waterfront space in warm seasons was set as 0.16 in CFD simulation. In the simulation, we set two settings for seasonal changes in the friction coefficients of the river and vegetation leaves in cold regions. In addition, in cold seasons, the grass was covered by snow, the river was frozen, and the emissivity of ice and snow was set as 0.98 in the MRT simulation. For warm seasons, the emissivity of the lawn was set to 0.78 and the emissivity of water was set to 0.96.

### 2.3. Simulation

Eddy3D invokes the OpenFOAM engine, which is suitable for studying outdoor thermal comfort [37,38]. Many researchers have used OpenFOAM to examine urban thermal comfort [39,40]. In this study, Eddy3D was employed to simulate wind speed, mean radiant temperature (MRT), and the universal thermal climate index (UTCI) in waterfront spaces.

#### 2.3.1. Mean radiant temperature (MRT)

$$T_{mrt} = \frac{\sum \varepsilon_i F_i (T_i)^4}{\sum \varepsilon_i F_i} \quad (1)$$

$T_{mrt}$  represents the mean radiant temperature,  $\varepsilon_i$  means the emissivity of surface,  $F_i$  is the angle factor between the test point and the surrounding surface,  $T_i$  is the surface temperature in the simulation, and i represents the surrounding surface number [38]. In this study, solar and shortwave radiation from water bodies, green spaces, vegetation, buildings, and roads were considered, and the surface emissivities of these materials are listed in Table 4.

#### 2.3.2. Computational fluid dynamics (CFD)

$$\frac{\partial \rho h}{\partial t} + \mathbf{u} \cdot \nabla(\rho h) + \rho \mathbf{u} \cdot \nabla \left( \frac{1}{2} \mathbf{u} \cdot \mathbf{u} \right) = -\nabla \cdot \mathbf{q} + S_H \quad (2)$$

$\rho$  means the fluid density,  $\mathbf{u}$  is the fluid velocity,  $\mathbf{q}$  is the thermal flux and  $S_H$  is a source term, which is used to include the solar radiation [41].

#### 2.3.3. Universal Thermal Climatic Index (UTCI)

$$UTCI = \int (T_a; T_{mrt}; \nu_{10}; RH; Met; Clo) = T_a + Offset(T_a; T_{mrt}; \nu_{10}; RH; Met; Clo) \quad (3)$$

$T_a$  is the air temperature,  $T_{mrt}$  means the mean radiant temperature,  $\nu_{10}$  is the air velocity at the height of 10 m,  $RH$  is the relative humidity,  $Met$  means the metabolic rate, and  $Clo$  represents the clothing insulation value [38].

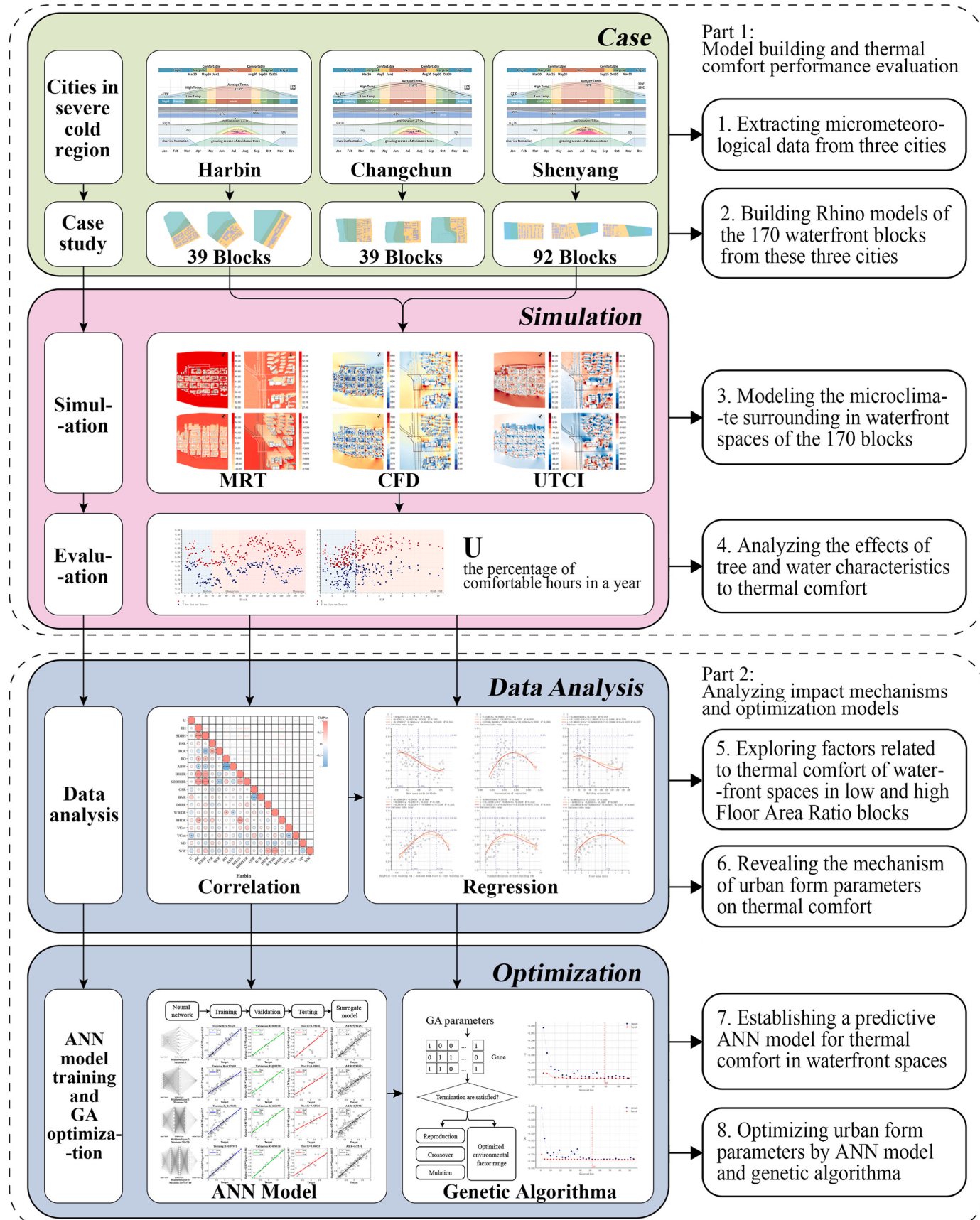


Fig. 1. Workflow of experiment and optimization procedure.



**Fig. 2.** 2Satellite images of case study.

**Table 1**  
Micrometeorological data of typical weather years.

	Harbin	Changchun	Shenyang
Location	Lon:126.68, Lat:45.72	Lon:125.22, Lat:43.90	Lon:123.45, Lat:44.70
Wind speed (m/s)	8.4	11.4	9.2
Air temperature (°C)	-26.9–28.8	-22.7–29.8	-21.0–31.7
Relative humidity (%)	10.6–98.2	15.0–105.2	57.0–84.0
Max. Direct normal radiation (Wh/m <sup>2</sup> )	983	781	938

#### 2.4. Performance indicator

$$U = \frac{\sum_{i=1}^N CU_i}{n \cdot N} = \frac{\sum_{i=1}^N CU_i}{5475} \quad (4)$$

$U$  is the relative comfort coefficient of waterfront spaces in cold regions,  $n$  is the number of simulation hours conducted within one day (based on activity habits in cold waterfront spaces,  $n = 15$ , representing 6:00 a.m. to 9:00 p.m.),  $N$  is the total number of simulation days (including four seasons, the  $N = 365$ ),  $CU_i$  is the number of comfortable hours (evaluated by the UTCI) in one day.

to 9:00 p.m.),  $N$  is the total number of simulation days (including four seasons, the  $N = 365$ ),  $CU_i$  is the number of comfortable hours (evaluated by the UTCI) in one day.

#### 2.5. Morphology parameters

Based on literature review and the UTCI formula, this study further refined several quantifiable factors influencing buildings, vegetation, and rivers.

##### 2.5.1. Building parameters

This research selects 13 building parameters and the formulas of them are shown below:

- The building height (BH) is the average building height of each block, and its formula is as follows:

$$BH = \frac{\sum_i^n h_i}{N} \quad (5)$$

As shown in Fig. 5 (1),  $h_i$  is the building height and  $N$  is the total number of buildings in one block.

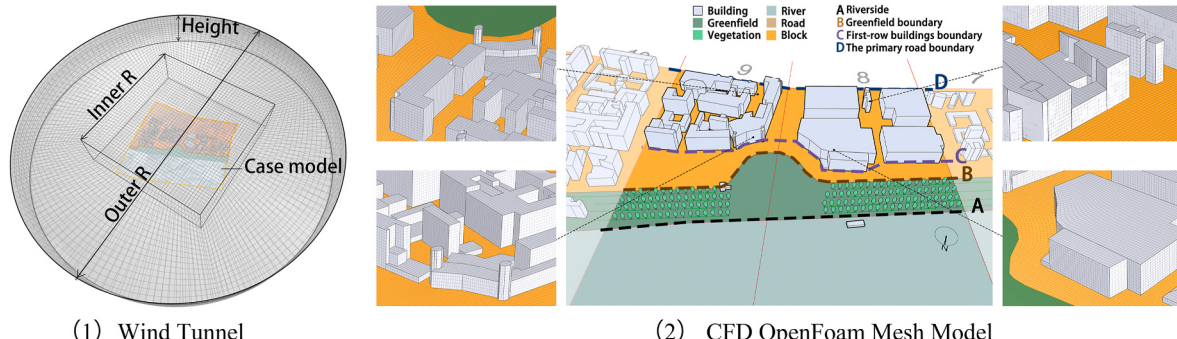


**Fig. 3.** 3Rhino digital model and OpenFoam CFD mesh model.

**Table**

2 Grid-independence analysis.

CFD mesh model	1	2	3	4	5	6	7	8	9
Block size	24	12	8	4	4	4	4	3	2
Inner R (meter)	15H	15H	15H	15H	25H	25H	25H	25H	25H
Outer R (meter)	40H	40H	40H	40H	40H	50H	40H	40H	40H
Height (meter)	5H								
Accuracy ( $R^2$ )	0.58	0.62	0.67	0.71	0.77	0.89	0.89	0.90	0.90
Runtime (min)	25	42	76	145	176	205	297	485	780

**Fig. 4.** Measurement in warm and cool seasons.**Table**

3 Measuring equipment parameter information.

Instrument	Meteorological parameter	Measuring Range	Accuracy
AZ87789	Air temperature ( $T_a$ )	-30 to +50 ( $^{\circ}\text{C}$ )	$\pm 0.6\ ^{\circ}\text{C}$
AZ87585	Relative humidity (RH)	0-100%	$\pm 0.1\%$
AZ87789	Black globe temperature ( $T_g$ , $\phi = 75\text{ mm}$ )	-10 to +80 ( $^{\circ}\text{C}$ )	$\pm 0.6\ ^{\circ}\text{C}$
Testo 450i	Air velocity ( $V$ )	0 to 30 (m/s)	$\pm 0.1\text{ m/s}$

- Standard deviation of building height (SDBH) is a measure that is used to quantify the amount of variation or dispersion of a set of building height.

$$SDBH = \sqrt{\frac{\sum_i^n (h_i - \bar{h})^2}{N}} \quad (6)$$

In Fig. 5 (2),  $h_i$  is the building height,  $\bar{h}$  is the average building height, and  $N$  is the total number of buildings per block. For the first building row, the height of the first building row (BH.FR) and standard deviation of the first building row (SDBH.FR) have the same calculation method.

**Table**

4 CFD parameter setting.

Simulation	Tools	Constant Items	City Harbin	City Changchun	City Shenyang
CFD OpenFoam		Air temperature range Wind speed range Wind direction Boundary type Boundary Inner rectangle Boundary Outer radius Boundary height Block size Mesh type CFD Turbulence model Pressure model Terrain roughness index of waterfront space in cold seasons (without leaves) Terrain roughness index of waterfront space in warm seasons (with leaves) Terrain roughness index of cities Concrete (emissivity of the surface) Asphalt (emissivity of the surface) Lawn (emissivity of the surface) Ice and snow (emissivity of the surface) Water (emissivity of the surface)	-26.9-28.8 $^{\circ}\text{C}$ 0-17 m/s $0^{\circ}, 45^{\circ}, 90^{\circ}, 135^{\circ}, 180^{\circ}, 225^{\circ}, 270^{\circ}$ and $315^{\circ}$ Cylindrical domain 25H 80H 5H 4 OpenFOAM's blockMesh and snappyHexMesh RealizableKE SIMPLE (Semi Implicit Method for Pressure Linked Equations) 0.12 0.16 0.22 0.95 0.92 0.78 0.98 0.96	-22.7-29.8 $^{\circ}\text{C}$ 0-20 m/s 0-17 m/s	-21.0-31.7 $^{\circ}\text{C}$
MRT EnergyPlus					

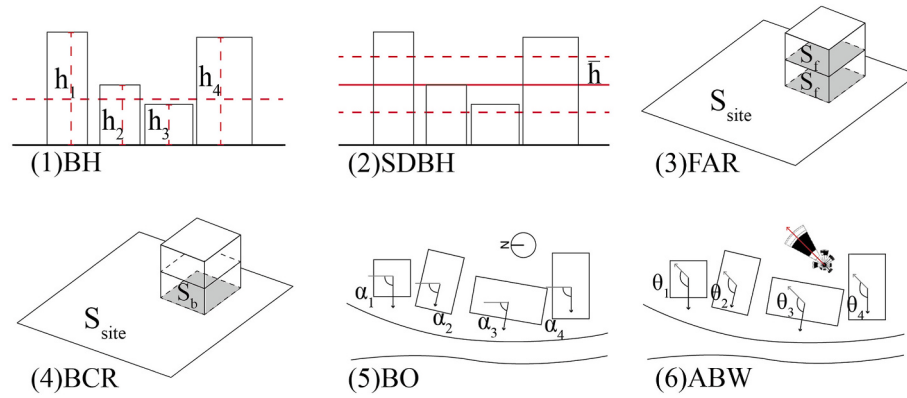


Fig. 5. 5Partial morphology parameters.

- The floor area ratio (FAR) is the relationship between the total amount of useable floor area that a building has, or has been permitted to have, and the total area of the lot on which the building stands. A higher ratio indicates dense or urban construction.

$$FAR = \frac{S_f}{S_{site}} \quad (7)$$

- Ratio of building area (BCR) to site area. Building area refers to the floor space of a building when looking down from the sky.

$$BCR = \frac{S_b}{S_{site}} \quad (8)$$

In Fig. 5 (3) and Fig. 5 (4),  $S_{site}$  means is the total area of the case study sites,  $S_f$  is the floor area, and  $S_b$  is the building projection area.

- Building orientation (BO) refers to how a building is positioned in relation to the path of the sun throughout the seasons and prevailing wind patterns.

$$BO = \frac{\sum_i^n \alpha_i}{N} \quad (9)$$

As shown in Fig. 5 (5),  $\alpha_i$  means angle between north and building orientation; N is the total number of buildings in one block.

- The angle between the building and prevailing wind (ABPW) reflects the angle between the main building facade and the prevailing wind direction.

$$ABPW = \frac{\sum_i^n \theta_i}{N} \quad (10)$$

As shown in Fig. 5 (6),  $\theta_i$  is the angle between north and building orientation, and N is the total number of buildings in one block.

- The Open Space Ratio (OSR) is generally the percentage of open area relative to the building floor area. However, in this study, this was calculated using the length ratio.

$$OSR = \frac{\sum_i^n l_i}{L_{total}} \quad (11)$$

As shown in SFig.9 (1),  $l_i$  is the void length between buildings, and  $L_{total}$  is the total length of the waterfront.

- Building to void ratio (BVR) is the ratio of the total building facade length to the total open area length.

$$BVR = \frac{\sum_i^n L_i}{\sum_i^n l_i} \quad (12)$$

As shown in SFig.9 (2),  $l_i$  is the void length between buildings,  $L_i$  is the total length of the waterfront.

- The distance from the river to the first building row (DRFR) is the average distance between different buildings in the first row and river boundary.

$$DRFR = \frac{\sum_i^n D_i}{N} \quad (13)$$

In SFig.9 (3),  $D_i$  is the distance between each building in the first row and the river boundary, and N is the total number of buildings.

- The ratio of the width of the waterfront to the distance between the river and the building ratio (WWDR) is the ratio of the width of the open space on the waterfront to the distance between the river boundary and the buildings in the first row.

$$WWDR = \frac{W_i}{D_i} \quad (14)$$

In SFig.9 (4),  $D_i$  is the distance between the buildings in the first row and the river boundary,  $W_i$  is the width of the open-space waterfront.

- The building height to distance between the river and the building ratio (BHDR) is the building height of the first row divided by the average distance between the different buildings in the first row and the river boundary.

$$BHDR = \frac{H_i}{D_i} \quad (15)$$

In SFig.9 (5),  $D_i$  is the distance between the buildings in the first row and the river boundary,  $H_i$  means building height in the first row.

### 2.5.2. Vegetation and river parameters

This study selected four vegetation and river parameters and their formulas are as follows:

- The width of the waterfront (WW) is the difference between the width of the open space on the waterfront and the distance between the center of each block and the river boundary.

$$WW = D_{bi} - W_i \quad (16)$$

As shown in SFig.9 (6),  $D_{bi}$  is the distance between every block center in the first row and the river boundary,  $W_i$  is the width of the open space waterfront.

- The vegetation coverage (VCov) is the percentage of vegetation in an area, which is the ratio of the canopy projection area to the gross lot area.

$$VCov = \frac{S_{canopy}}{S_{site}} \quad (17)$$

As shown in SFig.9 (7),  $S_{site}$  means is the total area of the case study sites and  $S_{canopy}$  is the canopy projection area.

- Vegetation concentration (VCon) is frequently used to measure the inequality in one variable over the distribution of another, which reflects the centrality of the vegetation positions.

$$VCov = \frac{n\sqrt{\frac{S_w}{S_{site}}}}{\sum_i^n d_{ci}} \quad (18)$$

As shown in SFig.9 (8),  $S_{site}$  means is the total area of the case study sites,  $S_w$  is the waterfront area, and  $d_{ci}$  is the distance between the trees and the center of the area.

- Vegetation distribution (VD) is the average distance between trees and river boundary.

$$VD = \frac{\sum_i^n d_i}{N_t} \quad (19)$$

As shown in SFig.9 (9),  $d_i$  is the distance between the trees and river boundary, and  $N_t$  is the total number of trees.

## 2.6. Machine learning

In this study, an ANN was used to construct a predictive model for increasing the number of data samples. As shown in Fig. 6, the input dataset was a matrix of several sub-environmental factors at the building, vegetation, and river levels. The MRT, CFD, UTCI, and U data from the measurements, simulations, and calculations were used to form a matrix as the output dataset.

$$\begin{aligned} h(k) &= \int_2 (w_2 \cdot x(k) + b_2) \\ x(k) &= \int_1 (w_1 \cdot u(k) + b_1) \end{aligned} \quad (20)$$

The output vector from the hidden layer is  $x(k)$ ,  $w_1$  is the connection weight matrix from the input to the hidden layer;  $w_2$  is the connection weight matrix from the hidden layer to the output layer;  $b_1$  and  $b_2$  denote the bias numbers in the hidden and output layers, respectively. The transfer algorithm used between the hidden and output layers is as follows:

$$\int(P) = \frac{1 - e^{-2P}}{l + e^{-2P}} \quad (21)$$

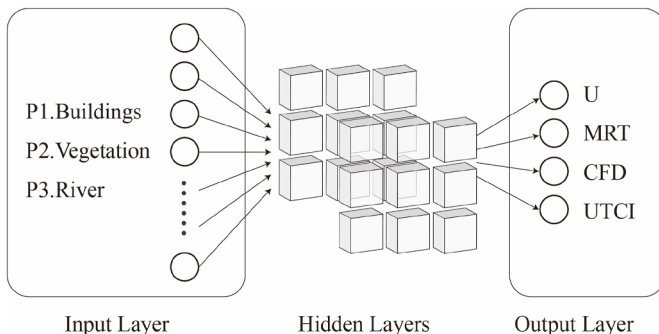


Fig. 6. Machine learning structures.

$P$  shows a function of

$$P = \int \left( \sum w_i x_i \right) \quad (22)$$

## 3. Results

### 3.1. Correlation factors

#### 3.1.1. Simulation result

To illustrate the influence of wind speed and MRT on the thermal comfort of the waterfront space in cold regions, we selected the typical coldest hour (December 15th 9 a.m.) and hottest hour (August 20th 2 p.m.) to analyze the wind, MRT, and UTCI cloud charts.

**3.1.1.1. Wind speed cloud charts.** As shown in Fig. 7 and SFig.10, the winter and summer wind speed cloud maps for typical hours in waterfront spaces with a high floor area ratio (FAR) and low FAR surrounding blocks are shown, from which it can be seen that the wind speed attenuates significantly after the wind flow passes through building groups and vegetation. From Fig. 7 and SFig.10, comparing the waterfront spaces with a high FAR surrounding block and those with a low FAR surrounding block, the wind speed decreased by 12%–31% in the waterfront spaces with a high FAR surrounding block, and the wind speed decreased by 6%–17% in the waterfront spaces with low FAR surrounding blocks. This means that, in both cold and warm seasons, a higher FAR of the surrounding blocks would decrease the wind speed in the waterfront spaces. To be more particular, the wind speed increasing by about 22% appeared at the first-row buildings' corner from the waterfront spaces, this is evident in the case with low FAR surrounding blocks. This causes wind speeds to increase significantly in the waterfront space near the corners of the first row of buildings.

From the analysis of tree influence, in summer, the wind speed increased by 16%–37% in the wind shadow area behind the tree. However, in winter, the increase in wind speed, which only increased by 3%–7%, in the space between the wind shadow areas, was much weaker than that in summer.

**3.1.1.2. MRT cloud charts.** As shown in Fig. 8 and SFig.11, the winter and summer MRT cloud maps for typical hours in high-FAR and low-FAR blocks are shown, from which it can be seen that shading by building groups and vegetation has a huge impact on the MRT, and that the impact of vegetation on the MRT decreases in winter due to leaf loss. From the analysis of the influence of buildings, the buildings' shadows could decrease the MRT by 27–46%, which is more influential in waterfront spaces with higher FAR surrounding blocks. However, the influence of buildings on MRT depends on the orientation of the surrounding blocks. As for the tree's influence, it is obvious that the dense trees in summer have more effects on MRT than that in winter.

**3.1.1.3. UTCI cloud charts.** The UTCI cloud charts for typical winter and summer hours in waterfront spaces with high and low FAR surrounding blocks are shown in Fig. 9 and SFig.12. From the analysis of building's effect, in summer, the waterfront spaces with high FAR surrounding block have higher UTCI than that with low FAR surrounding block. This might be because the wind speed was higher in the waterfront spaces with low FAR surrounding blocks, which could also mean that wind speed had a greater influence on the thermal comfort of waterfront spaces in the summer. In winter, large shaded areas in waterfront spaces decrease the UTCI dramatically, and this appears obvious in waterfront spaces with high FAR surrounding blocks. In addition, as the waterfront spaces are not shielded by enclosed buildings, the shaded areas of the high FAR block have a strong impact on thermal comfort in winter. However, because trees have no leaves in winter, the influence of trees on the thermal comfort of waterfront spaces is stronger in summer.

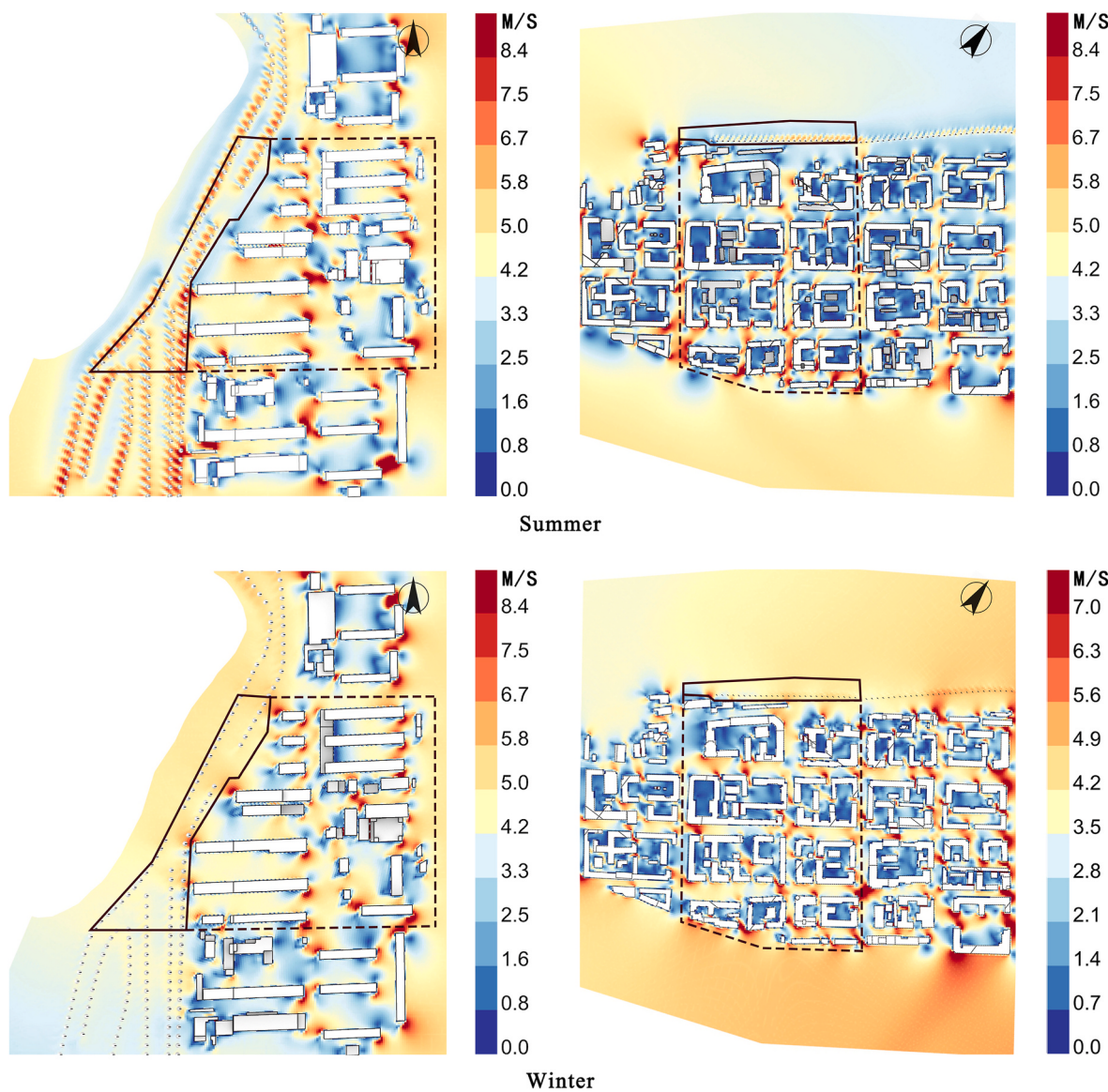


**Fig. 7.** 7Wind speed cloud charts in high FAR block.

### 3.1.2. U-value

**3.1.2.1. Effects of special tree–water states on U in cold regions.** As shown in Fig. 10 (1), the distribution of U in different blocks can be seen from the scatter plot, with the red scatter indicating that the special tree–water characteristics of cold regions (river freezing and leaf fall in winter) were considered, and the blue scatter indicating that these characteristics were not included. The first 39 blocks were from Harbin, the second 39 from Changchun, and the last 92 from Shenyang. From the results, it can be seen that considering tree–water features is necessary in cold regions, and the thermal comfort performance improves after considering tree–water, with differences ranging from 2% to 15%. In addition, the thermal comfort of waterfront spaces in cold regions gradually increases as the latitude of the city decreases, which is consistent with the results of a previous study on outdoor thermal comfort [42].

**3.1.2.2. Effects of tree–water status on U in different FAR blocks.** As shown in Fig. 10 (2), the distribution of U in the high- and low-FAR blocks can be observed in the scatter plots with and without considering the tree–water features of the cold region. The high FAR blocks

have more thermal comfort hours than the low FAR blocks, with 16% more thermal comfort hours accounted for. Both blocks performed better in terms of thermal comfort when tree–water features were considered, and this difference was more pronounced in the high-FAR block.

Overall, as emphasized in previous studies [19], tree–water characteristics specific to cold regions (river ice and leaf fall in winter) have a significant impact on thermal comfort and must be considered in simulations.

### 3.1.3. Correlation analysis

**3.1.3.1. Correlation analysis of U and influence factors in two cities.** SFig.13 shows the results of the Pearson correlation analysis between U and the 17 influencing factors. In Harbin, U is significantly correlated (\* indicates significance) with VCon. In Changchun, U significantly correlated with ABW, OSR, BVR, DRFR, and VD. In Shenyang, U significantly correlated with SDBH.FR and VCov.

**3.1.3.2. Correlation analysis of U and influence factors in two types of blocks.** The results of the Pearson correlation analysis of U and 17

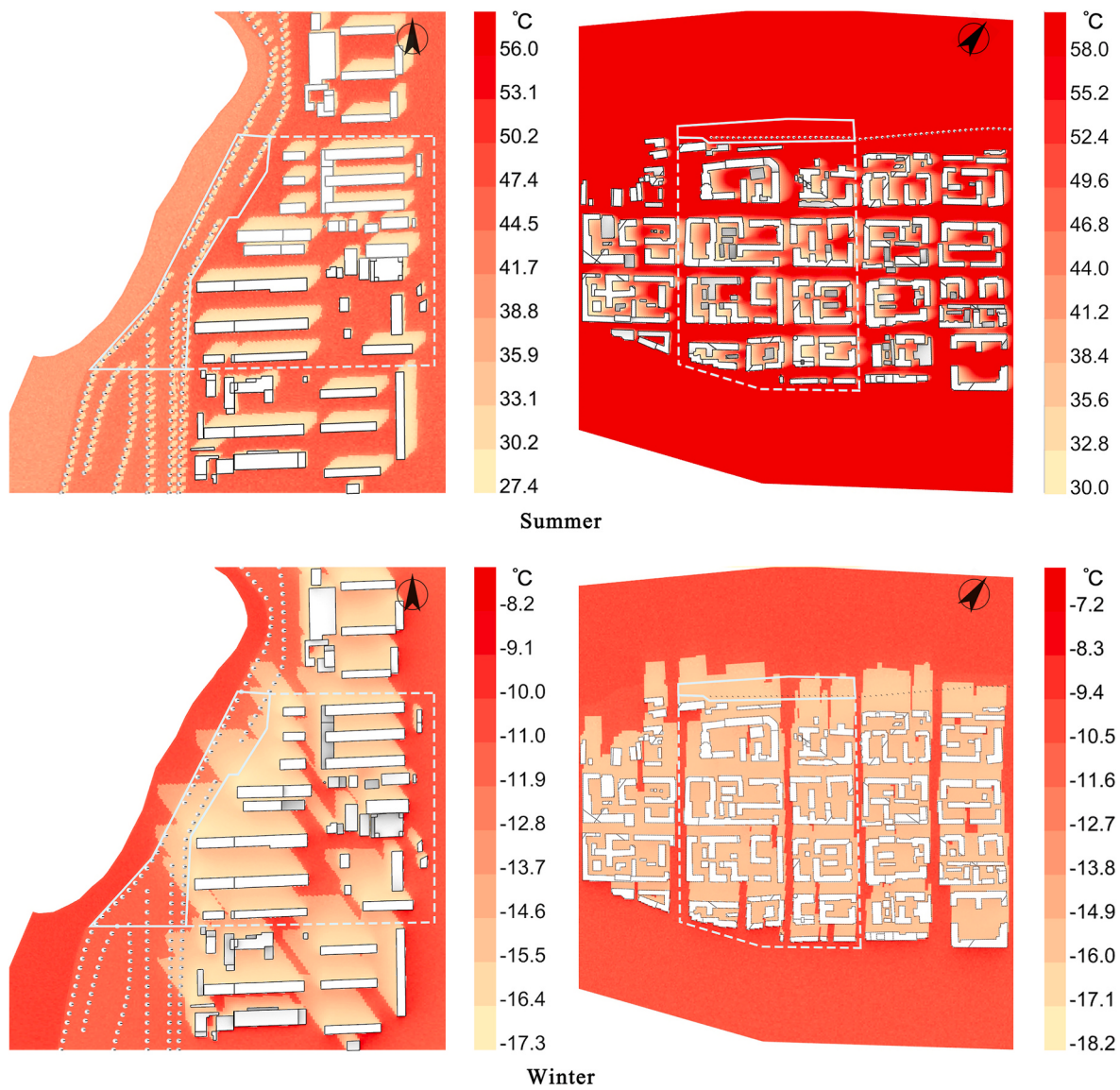


**Fig. 8.** 8MRT cloud charts in high FAR block.

influencing factors in both the high and low FAR blocks are shown in Fig. 11. It can be seen that U in high FAR blocks is significantly correlated (\* indicates significance) with SDBH, BCR, BO, ABW, BH.FR, SDBH.FR, OSR and BHDR. In addition, U in the low-FAR block was significantly correlated with SDBH, BO, ABW, SDBH.FR, BH, BH.FR, and OSR.

In general, the influencing factors significantly associated with thermal comfort in the waterfront spaces were VCon, ABW, OSR, BVR, DRFR, VD, SDBH, BCR, BO, SDBH.FR, and BHDR. In addition, as the correlation analyses of high and low FAR blocks show more regularity, this suggests that FAR has a non-negligible influence on the mechanisms of U. Among these factors, there is a strong autocorrelation among VCon, VCov, and VD, and between ABW and BO, OSR and BVR, DRFR and BHDR, SDBH and SDBH.FR, BCR, and FAR. After screening out the autocorrelation factors, six correlation factors, namely VCon, BO, OSR, SDBH.FR, FR, BHDR, and FAR, were retained to further explore their influence on U. Factors such as BO, FAR, and SDBH.FR have been mentioned in previous studies on waterfront thermal comfort, and the present study corroborates these results while expanding on the influencing factors [17,43].

### 3.2. Influence mechanisms

#### 3.2.1. Building orientation (BO) and floor area ratio (FAR)

As shown in Fig. 12 (1) and SFig.14 in fit of U with BO, U decreases with increasing BO when BO is between 0° and 110°, and increases when it is between 110° and 180°. A similar pattern was observed in the low-FAR blocks, whereas in the high-FAR blocks, U continued to decrease as BO increased. A possible reason might be that blocks where the BO is approximately 110° are located on the north bank of the river, while the dominant wind direction in winter cities is south and southwest; therefore, the waterfront space is directly exposed to cold winds. Another reason might be that waterfront buildings closest to the north bank frequently present low heights and FAR, considering the overall lighting of the blocks; thus, the buildings have less blocking effect on the wind. High wind speeds resulted in low thermal comfort. A previous study showed that thermal comfort was better when buildings or riverbanks faced a certain direction [20]. In this work, U is relatively high in high FAR blocks when BO is between 14.7 and 57.9, with a maximum value of 0.363, while U is relatively high in low FAR blocks when BO is between 12.95 and 167.43, with a maximum value of 0.331.

As shown in Fig. 12 (2) and SFig.15, for the fit of U with the floor area ratio (FAR), U increased with FAR. This was also verified in another

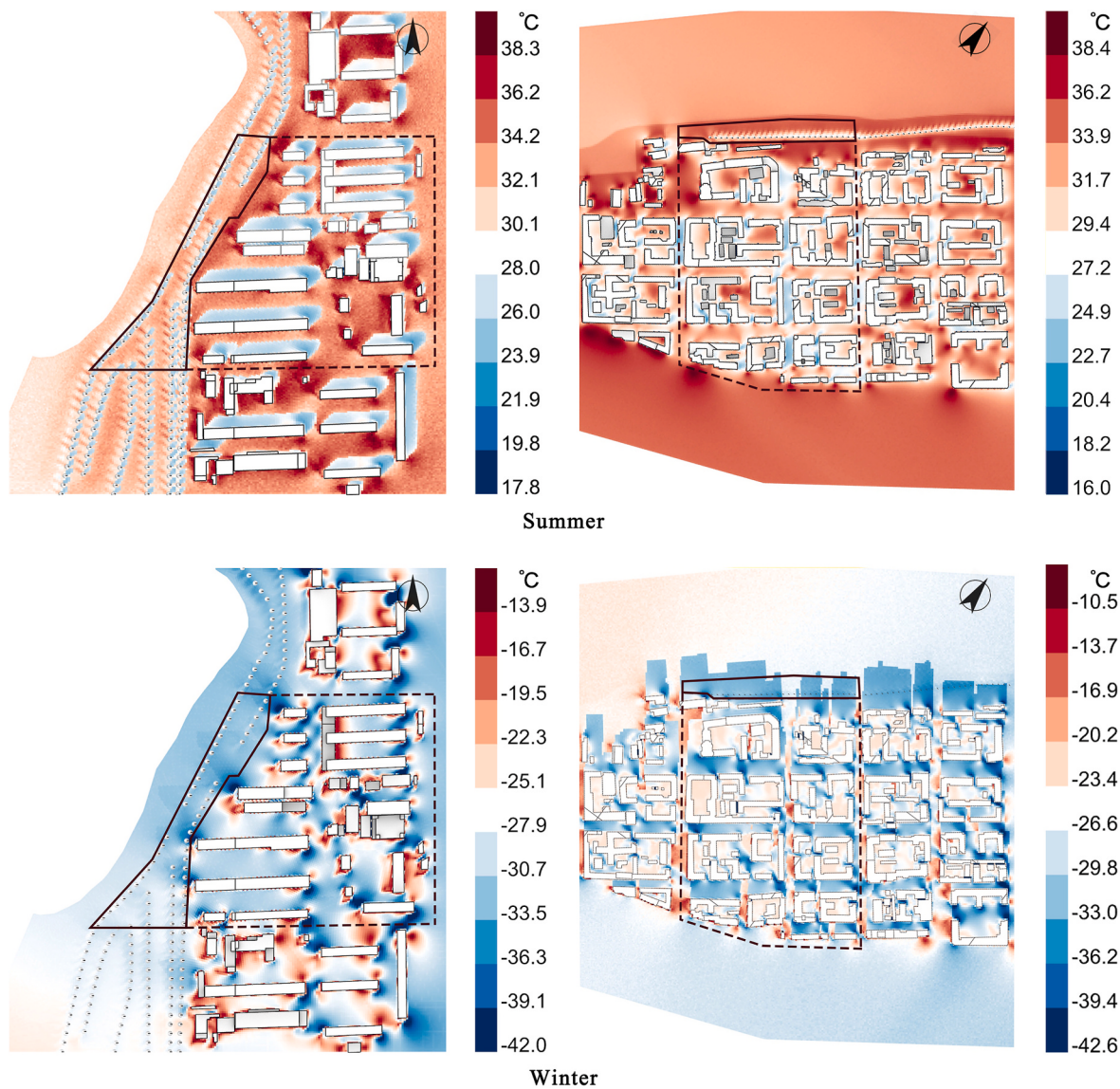


**Fig. 9.** 9UTCI cloud charts in high FAR block.

study on waterfront environments [21]. A similar pattern occurs in high-FAR blocks ( $\text{FAR} > 3$ ), whereas in low-FAR blocks ( $\text{FAR} < 3$ ),  $U$  decreases with increasing FAR when FAR is between 0 and 1.25, then increases when FAR is greater than 1.25. The possible reasons for this are that waterfront blocks with FAR less than 1.25 are less likely to be found on the south shore owing to land use and daylighting norms, buildings have less impact on solar radiation in the waterfront space, and because of the bypassing effect of south-facing winds. As the FAR increases, the wind speed flowing through the two sides increases, leading to a reduction in thermal comfort. Thermal comfort increased with an FAR greater than 1.25, an increase in the plot ratio, a greater proportion distributed on the south shore, and a more obvious blocking effect of the southward-dominant wind by the building.  $U$  was relatively high in the high-FAR blocks when the FAR was between 3.25 and 7.58, and in the low-FAR blocks when the FAR was between 0.475 and 2.785. In general,  $U$  is higher in the high-FAR blocks than in the low-FAR blocks.

### 3.2.2. Open space ratio (OSR), BHDR and SDBH.FR

As shown in Fig. 13 (1) and SFig.16 in fit of  $U$  about open space ratio (OSR),  $U$  decreases as OSR increases when OSR is between 0 and 0.7, increases as OSR increases when OSR is between 0.7 and 1. This trend was

observed for both high- and low-FAR blocks, whereas the effect of OSR on  $U$  was more pronounced for the low-FAR blocks. This may be because as the OSR increases, the open space becomes a channel for wind bypass flow, and the increase in wind speed decreases thermal comfort, whereas when the OSR approaches 1, the wind speed approaches the original speed, and the decrease in wind speed increases thermal comfort.  $U$  is relatively high when OSR is between 0.0025 and 0.3884 in high FAR blocks, and between 0.06 and 0.47 in low FAR blocks.

As shown in Fig. 13 (2) and SFig.17,  $U$  increases with increasing BHDR between 0 and 0.6, and decreases with increasing BHDR between 0.6 and 1. This pattern is more pronounced in the low-FAR blocks, whereas in the high-FAR blocks,  $U$  increases as BHDR increases. A possible reason for this is that as the BHDR increases, the wind shadow zone created by buildings in the waterfront space also increases, and a reduction in wind speed leads to increased thermal comfort. In contrast, in low-FAR blocks, when the BHDR exceeds 0.6, the OSR is likely to be large, increasing the wind bypass and wind speed and reducing thermal comfort.  $U$  is relatively high when the BHDR is between 0.2685 and 0.7158 in the high-FAR blocks, and between 0.2378 and 0.674 in the low-FAR blocks.

As shown in Fig. 14 (1) and SFig.18 in the fitting of  $U$  about standard deviation of the first building row (SDBH.FR),  $U$  increases gradually

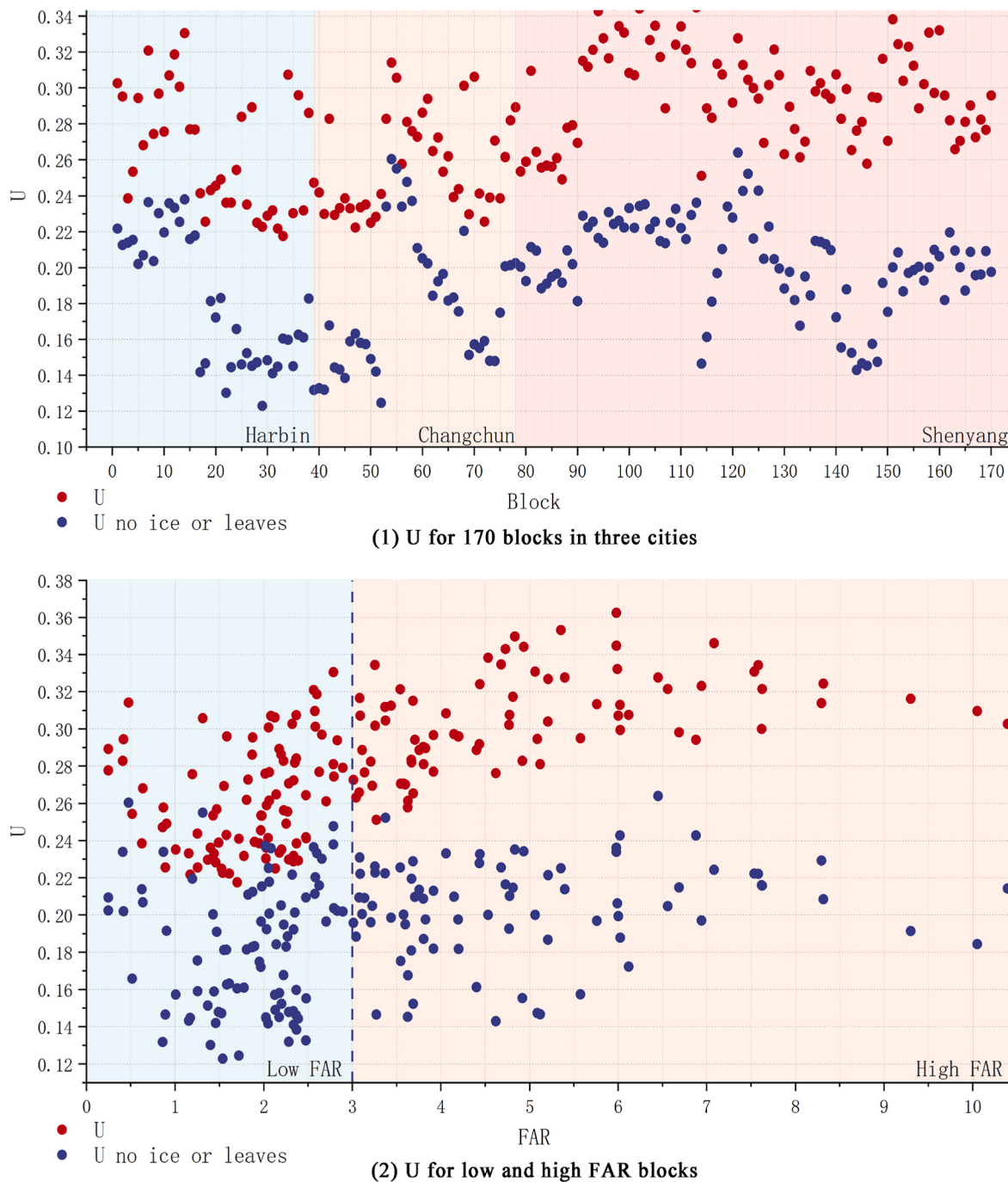


Fig. 10. 10Scatter plot of U for different blocks.

with SDBH.FR. This was more evident in low-FAR blocks, whereas in high-FAR blocks, U decreased with increasing SDBH.FR when SDBH.FR was greater than 30. A possible reason for this may be an increase in SDBH.FR implies an increase in the building height, wind shadow zone, and thermal comfort, whereas when the BH reaches a certain level, the narrow tube effect begins to appear on the ground near the high-rise building, and the increase in wind speed leads to a decline in thermal comfort. U is relatively high when SDBH.FR is between 17.6 and 58.3, respectively, in the high-FAR blocks and between 0 and 54.73 in the low-FAR blocks.

### 3.2.3. Vegetation concentration (VCon)

As shown in Fig. 14 (2) and SFigs.19 in fit of U with vegetation concentration (VCon), U increases with incremental VCon. A similar pattern

was observed in both the high- and low-FAR blocks, with greater variation in U in the low-FAR blocks. This is probably because a more concentrated distribution of vegetation provides more effective summer shade, and the positive impact of shading in summer on thermal comfort is greater than the negative impact of wind blocking. U is relatively high when VCon is between 0.0014 and 0.0027 in the high-FAR blocks and between 0.00121 and 0.00365 in the low-FAR blocks.

### 3.3. Optimization

#### 3.3.1. Thermal comfort prediction model

As shown in Fig. 15 and SFigs.20–22, this study trained four artificial neural network (ANN) prediction models with different numbers of hidden layers and neurons and compared their prediction performance

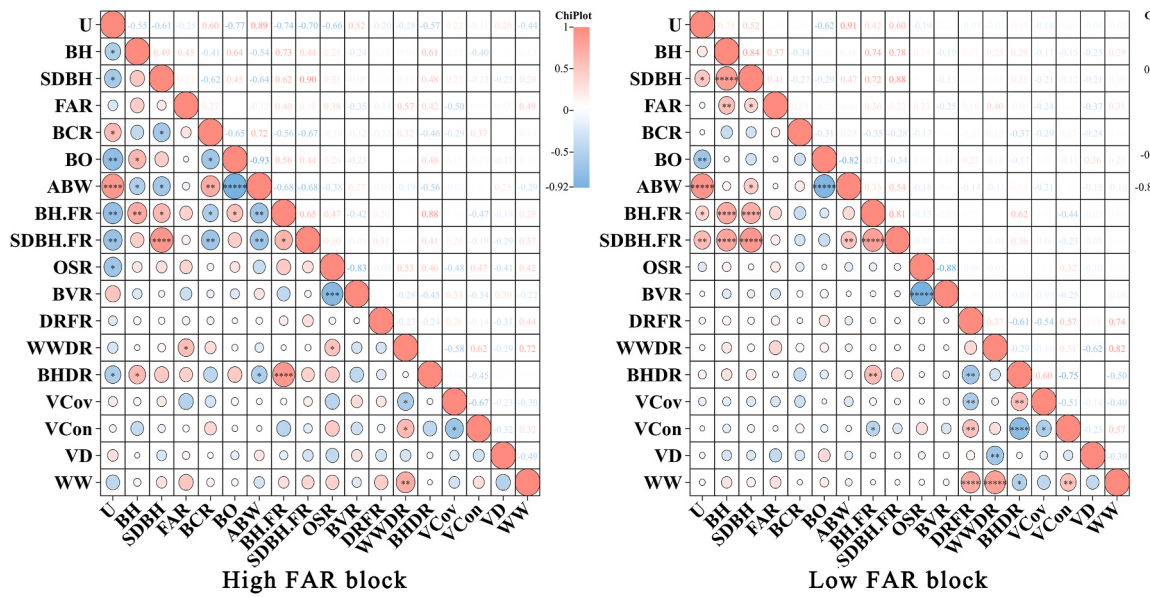
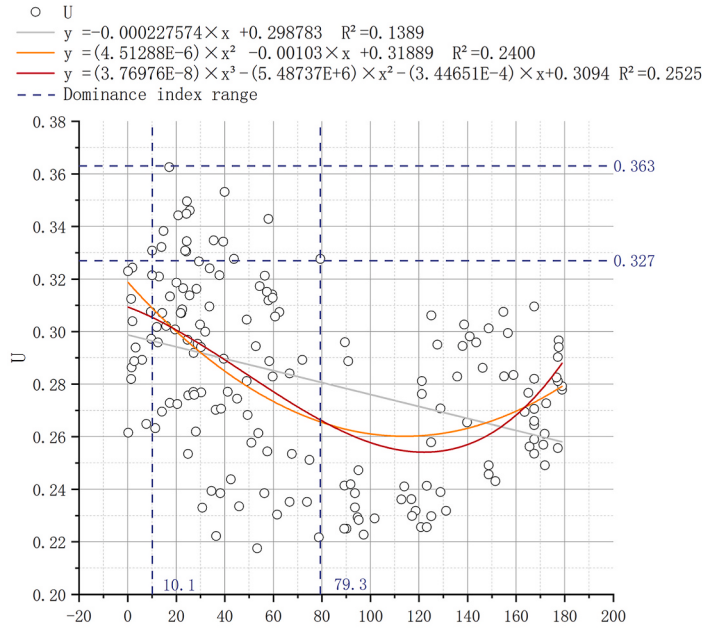
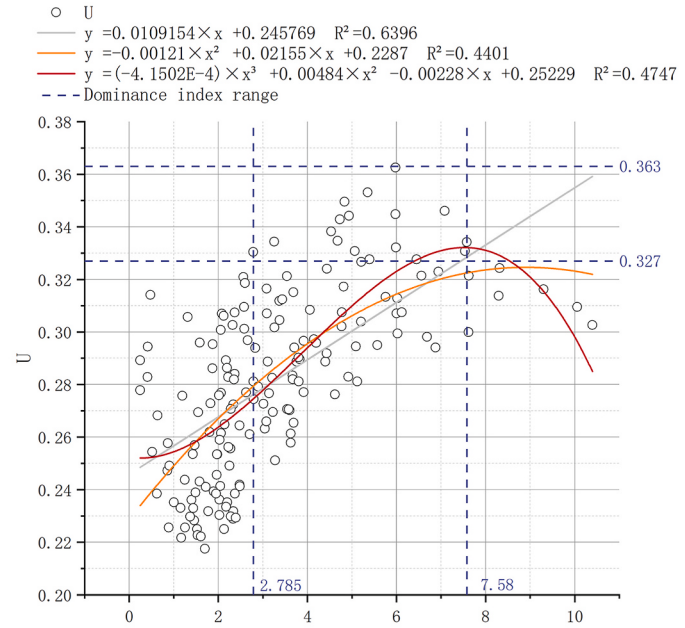


Fig. 11. Correlation analysis between U and influence factors in high and low FAR blocks.



(1) U and building orientation



(2) U and floor area ratio

Fig. 12. Regression analysis between U and BO, and U and FAR.

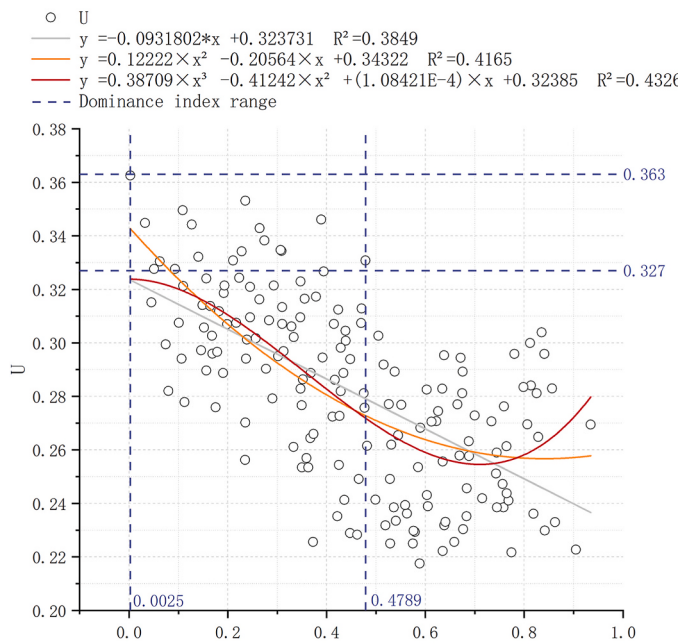
based on U and six influence factor data from 170 blocks. The ANN model with three hidden layers containing 15 neurons each was found to be the most accurate in predicting waterfront thermal comfort, with the prediction accuracy of 95.76%.

Although the ANN model has been applied to urban thermal comfort research [28], not all neural network structures were suitable for another study that compared and screened the structures of neural networks, and the resulting neural networks were adopted for the optimization of urban form parameters in waterfront neighborhoods.

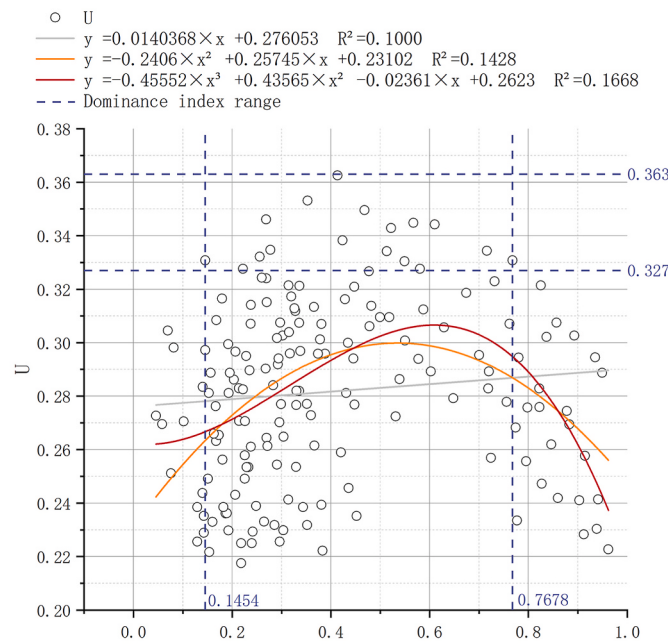
### 3.3.2. Optimization of urban morphology parameters in blocks

The process and results of the ANN combined with the GA for the optimization of six waterfront block cases (low and high FAR blocks

from Harbin, Changchun and Shenyang) are listed in Table 5 and SFigs.23–28. In the optimization process, the building orientation (BO) is kept constant by the relative position of the block and riverbank, the FAR can be varied within the range of the corresponding category (high or low FAR), and the other four parameters can be varied within the range of normative provisions and research pick-ups. The optimization results show that waterfront blocks in the same city have similar optimization effects and urban morphology trends. In Harbin, the low- and high-FAR block cases were optimized to improve thermal comfort by 22% and 7%, respectively, and both were optimized to increase the FAR, BHDR, and SDBH.FR, and to reduce the OSR. In Changchun, the low- and high-FAR block cases were optimized to improve thermal comfort by 77% and 106%, respectively, and both increased the SDBH.FR and

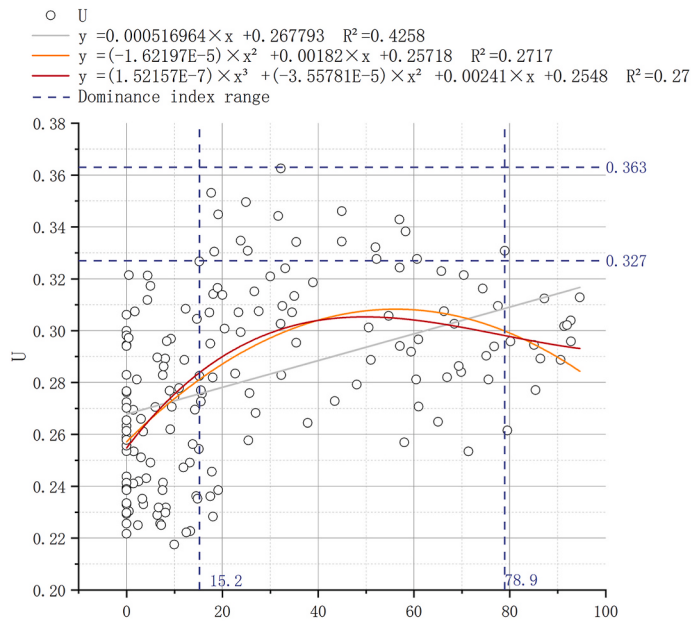


(1) U and open space ratio

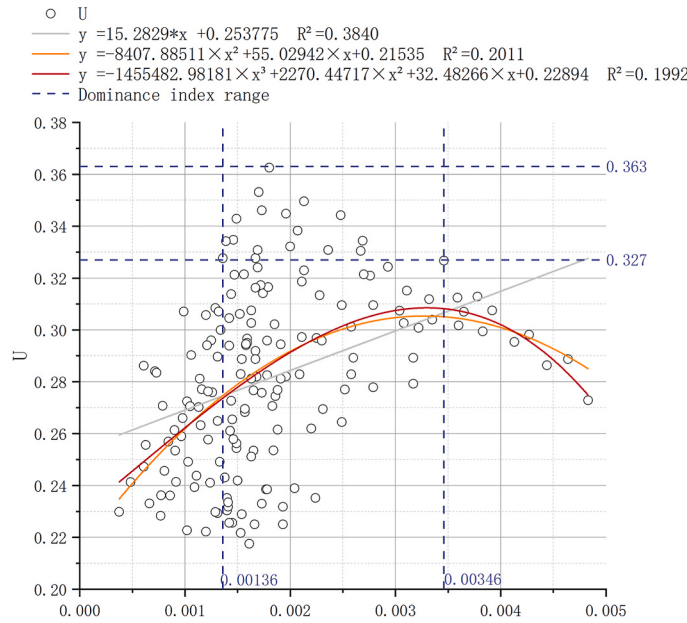


(2) U and BHDR

Fig. 13. Regression analysis between U and OSR, and U and BHDR.



(1) U and SDBH.FR



(2) U and vegetation concentration

Fig. 14. Regression analysis between U and SDBH.FR, and U and vegetation concentration.

decreased the FAR, OSR, and BHDR during the optimization process. In Shenyang, both low- and high-FAR block cases were optimized to improve thermal comfort by 3%, enhance BHDR and VCon, and reduce FAR and OSR. In comparison, the classification based on high or low FAR did not have as many common features as the urban classification. This is probably because climatic, historical, and normative differences result in each city's waterfront block form having its own characteristics. Thus, even if they fall into the same FAR category and follow similar mechanisms of thermal comfort impacts, the aspects that need to be optimized differ.

#### 4. Discussion

The research gaps in waterfront thermal comfort in cold regions were addressed above; however, three limitations of this study should be discussed.

##### 4.1. Limitations of research sample and simulation experiments

This case study is limited to a sample of four blocks in three cold regional cities. However, cold regions are extensive and urban

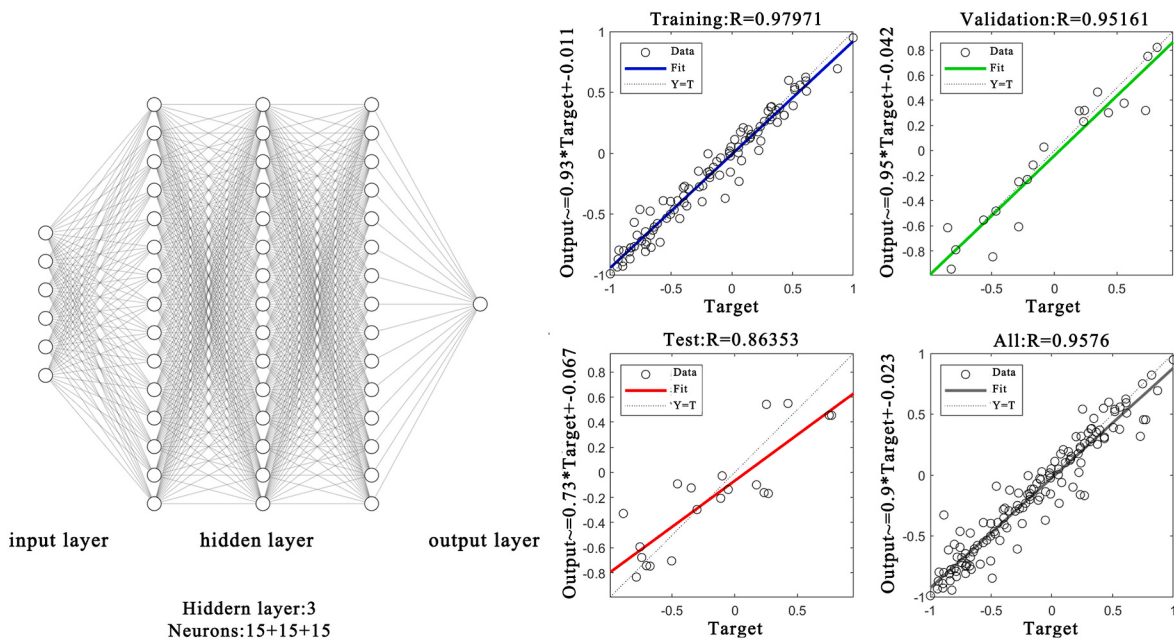


**Fig. 15.** ANN models with 3 layers and 15 neurons, and validation results.

morphologies may have different characteristics [44,45]. Further research is required to expand the number and distribution of cities. In addition, special winter tree–water characteristics in cold regions were considered in the simulation, and seasonal differences were reflected in different friction coefficients and solar radiation reflectivity. However, air temperature changes caused by water evaporation [16,46] and ice sublimation were not considered in this study and should be considered in further studies. Finally, the UTCI was regarded as a thermal assessment index in this study, which takes the wind speed at 10 m above the ground as the meteorological input variable and uses a relatively simple method to calculate the vertical wind profile under neutral steady conditions; in principle, micrometeorological flow conditions are not considered in urban buildings. Although the UTCI is now heavily used in the field of outdoor thermal comfort [47], future research is necessary for comparison with thermal indices, such as PET, mPET, and PT, to analyze the differences caused by this limitation.

#### 4.2. Limitations of excavating influence mechanisms

In this study, the thermal comfort metric U was used to characterize the thermal comfort of waterfront spaces, and its correlates and influence mechanisms were explored through simulation, correlation analysis, and regression analysis in sections 3.1 and 3.2. Some studies have shown that the urban form first affects the outdoor thermal comfort by altering the wind speed and MRT [48], which were included in our calculation of U in Section 2.3. However, this study did not quantitatively analyze how urban form affects wind speed and MRT or their mechanism of action on waterfront thermal comfort [37]. This issue should be addressed in future studies. This study focuses on the mechanisms by which urban form influences waterfront thermal comfort, with more attention to its impact on the outdoor environment. In fact, outdoor thermal comfort studies are also relevant to improving indoor environments: it can help to design the exterior spaces more adapted to the natural environment, reducing reliance on air-conditioning and heating systems, which can have a direct impact on buildings' energy efficiency and maintenance of indoor thermal comfort [49,50]. Besides, thermal comfort in the outdoor environment impact people's heat perception when moving from outdoors to indoors and drastic temperature differences will lead to discomfort [51]. Understanding outdoor thermal comfort is critical to regulating indoor temperature settings to

improve the comfort of transition [52].

#### 4.3. Limitations of concern perspectives

In this study, a machine learning prediction model for waterfront thermal comfort in cold regions was established based on an Artificial Neural Network (ANN), as described in Section 3.3. The ANN could quickly predict thermal comfort by simply inputting six urban form parameters of the waterfront blocks. A set of urban-form parameter optimization methods for waterfront blocks was also created based on ANN and GA, which can provide a reference for the range of urban-form parameters in design. However, this method cannot provide a specific optimized design solution, which may be achieved using a Generative Adversarial Network (GAN) model in the future [53].

## 5. Conclusions

In this study, the influence of seasonal changes in tree water characteristics on waterfront thermal comfort was investigated in cold regions. The urban form factors affecting thermal comfort in waterfront spaces were screened, and their influence was explored. Accordingly, an ANN-based prediction model was established for waterfront thermal comfort as well as an ANN-GA-based optimization model for urban form parameters in waterfront blocks, and a set of thermal comfort-oriented optimization design methods for waterfront blocks in cold regions was innovatively proposed. The conclusions are as follows:

- It is necessary to consider seasonal variations in tree–water characteristics in studies on waterfront thermal comfort in cold regions, which may affect the results by as much as 15%.
- BO, FAR, OSR, BHDR, SDBH.FR, and VCon are the six urban factors that influence the thermal comfort of waterfronts in cold cities. They show different mechanisms of influence in the high and low FAR blocks.
- The established ANN-based machine learning prediction model accurately predicts the thermal comfort of waterfront spaces, with the accuracy of 95.76%.
- The established ANN-GA-based optimization model of urban form parameters for waterfront blocks can effectively enhance waterfront

**Table 5** Optimization of urban morphology parameters.

A. Harbin low FAR block								B. Harbin high FAR block							
	Original	1	2	3	...	Best	Trend		Original	1	2	3	...	Best	Trend
<b>BO</b>	51.10	—	—	—	—	—	—	<b>BO</b>	40.54	—	—	—	—	—	—
<b>FAR</b>	2.207	2.748	2.991	2.962	...	3.000	↑	<b>FAR</b>	4.527	9.172	10.000	10.000	...	9.862	↑
<b>OSR</b>	0.278	0.304	0.060	0.045	...	0.003	↓	<b>OSR</b>	0.240	0.100	0.154	0.154	...	0.176	↓
<b>BHDR</b>	0.142	0.925	0.925	0.923	...	1.000	↑	<b>BHDR</b>	0.277	0.536	0.350	0.350	...	0.401	↑
<b>SDBH.FR</b>	16.890	90.143	90.143	90.143	...	100.000	↑	<b>SDBH.FR</b>	19.009	96.343	96.377	96.377	...	100.000	↑
<b>VCon</b>	0.001453	0.001604	0.001604	0.001604	...	0.001604	↑	<b>VCon</b>	0.001198	0.001805	0.000955	0.000955	...	0.001199	—
<b>U</b>	0.331	0.391	0.400	-0.4	...	0.403	22%	<b>U</b>	0.317	0.335	0.339	0.339	...	0.339	7%
<b>C. Changchun low FAR block</b>								<b>D. Changchun high FAR block</b>							
	Original	1	2	3	...	Best	Trend		Original	1	2	3	...	Best	Trend
<b>BO</b>	62.49	—	—	—	—	—	—	<b>BO</b>	90.87	—	—	—	—	—	—
<b>FAR</b>	2.260	0.858	0.858	0.858	...	0.250	↓	<b>FAR</b>	4.402	4.246	3.668	3.668	...	3.000	↓
<b>OSR</b>	0.415	0.316	0.316	0.316	...	0.285	↓	<b>OSR</b>	0.652	0.018	0.181	0.181	...	0.106	↓
<b>BHDR</b>	0.437	0.486	0.486	0.486	...	0.403	↓	<b>BHDR</b>	0.482	0.046	0.409	0.409	...	0.264	↓
<b>SDBH.FR</b>	3.385	22.648	22.648	22.648	...	7.166	↑	<b>SDBH.FR</b>	51.000	39.971	90.046	90.046	...	81.759	↑
<b>VCon</b>	0.000903	0.002904	0.002904	0.002904	...	0.003362	↑	<b>VCon</b>	0.001540	0.002966	0.001518	0.001518	...	0.001762	↓
<b>U</b>	0.179	0.312	0.312	0.312	...	0.316	77%	<b>U</b>	0.149	0.299	0.302	0.302	...	0.307	106%
<b>E. Shenyang low FAR block</b>								<b>F. Shenyang high FAR block</b>							
	Original	1	2	3	...	Best	Trend		Original	1	2	3	...	Best	Trend
<b>BO</b>	123.24	—	—	—	—	—	—	<b>BO</b>	134.89	—	—	—	—	—	—
<b>FAR</b>	2.480	2.471	1.670	2.471	...	0.749	↓	<b>FAR</b>	6.941	3.995	3.995	3.995	...	4.538	↓
<b>OSR</b>	0.436	0.188	0.118	0.188	...	0.003	↓	<b>OSR</b>	0.347	0.097	0.045	0.045	...	0.003	↓
<b>BHDR</b>	0.153	0.730	0.717	0.730	...	0.730	↑	<b>BHDR</b>	0.732	0.832	0.757	0.757	...	0.841	↑
<b>SDBH.FR</b>	0	12.311	18.107	0.188	...	0	—	<b>SDBH.FR</b>	65.727	9.764	32.473	32.473	...	31.918	↓
<b>VCon</b>	0.001502	0.004939	0.004642	0.004939	...	0.004962	↑	<b>VCon</b>	0.001560	0.003730	0.003730	0.003730	...	0.003914	↑
<b>U</b>	0.436	0.434	0.436	0.440	...	0.448	3%	<b>U</b>	0.347	0.349	0.349	0.351	...	0.357	3%

- thermal comfort by up to 106% of the year-round thermal comfort time.
- A waterfront block optimization design methodology combining simulation data with machine learning models is proposed, which can accurately and quickly optimize urban form parameters with the goal of thermal comfort to assist urban designers in making more rational decisions.

#### CRediT authorship contribution statement

**Jiayang Jiang:** Writing – review & editing, Writing – original draft, Visualization, Software, Project administration, Investigation, Formal analysis, Data curation, Conceptualization. **Wente Pan:** Writing – review & editing, Supervision, Resources, Project administration, Funding acquisition, Conceptualization. **Ruinan Zhang:** Writing – review & editing, Visualization, Validation, Software, Methodology, Formal analysis, Conceptualization. **Yang Hong:** Writing – original draft, Visualization, Software, Methodology, Conceptualization. **Jixian Wang:** Writing – original draft, Visualization, Software, Methodology, Investigation, Conceptualization.

#### Declaration of competing interest

We declare that we have no financial and personal relationships with other people or organizations that can inappropriately influence our work, there is no professional or other personal interest of any nature or kind in any product, service or company that could be construed as influencing the position presented in the manuscript entitled.

#### Data availability

Data will be made available on request.

#### Acknowledgements

The authors acknowledge that this research project was funded by the National Natural Science Foundation of China (Grant No. 52308017) and the China Postdoctoral Science Foundation (Grant No. 2022M710961).

#### Appendix A. Supplementary data

Supplementary data to this article can be found online at <https://doi.org/10.1016/j.buildenv.2024.111515>.

#### References

- [1] V.J. Lee, M. Ho, C.W. Kai, X. Aguilera, D. Heymann, A. Wilder-Smith, Epidemic preparedness in urban settings: new challenges and opportunities, *Lancet Infect. Dis.* 20 (5) (2020) 527–529.
- [2] U. Nations, Revision of World Urbanization Prospects, United Nations, New York, NY, USA, 2018, p. 799.
- [3] T. Xi, H. Qin, W. Xu, T. Yang, C. Hu, C. Zhao, H. Wang, Constantly tracking and investigating people's physical, psychological, and thermal responses in relation to park strolling in a severe cold region of China—a case study of stalin waterfront park, *Sustainability* 15 (9) (2023) 7043.
- [4] L. Lottrup, P. Grahn, U.K. Stigsdotter, Workplace greenery and perceived level of stress: benefits of access to a green outdoor environment at the workplace, *Landsc. Urban Plann.* 110 (2013) 5–11.
- [5] K.M. Korppala, T. Klemettlä, J.K. Hietanen, Evidence for rapid affective evaluation of environmental scenes, *Environ. Behav.* 34 (5) (2002) 634–650.
- [6] J.A. Hipp, G.B. Gulwadi, S. Alves, S. Sequeira, The relationship between perceived greenness and perceived restorativeness of university campuses and student-reported quality of life, *Environ. Behav.* 48 (10) (2016) 1292–1308.
- [7] H. Nordh, C. Alalouch, T. Hartig, Assessing restorative components of small urban parks using conjoint methodology, *Urban For. Urban Green.* 10 (2) (2011) 95–103.
- [8] M. Triguero-Mas, P. Dadvand, M. Cirach, D. Martínez, A. Medina, A. Mompart, X. Basagana, R. Gražulevičienė, M.J. Nieuwenhuijsen, Natural outdoor environments and mental and physical health: relationships and mechanisms, *Environ. Int.* 77 (2015) 35–41.
- [9] J. Maas, S.M. Van Dillen, R.A. Verheij, P.P. Groenewegen, Social contacts as a possible mechanism behind the relation between green space and health, *Health Place* 15 (2) (2009) 586–595.
- [10] T. Takano, K. Nakamura, M. Watanabe, Urban residential environments and senior citizens' longevity in megacity areas: the importance of walkable green spaces, *Journal of Epidemiology & Community Health* 56 (12) (2002) 913–918.
- [11] S. Chan, C.K. Chau, T. Leung, On the study of thermal comfort and perceptions of environmental features in urban parks: a structural equation modeling approach, *Build. Environ.* 122 (2017) 171–183.
- [12] L. Chen, Y. Wen, L. Zhang, W.-N. Xiang, Studies of thermal comfort and space use in an urban park square in cool and cold seasons in Shanghai, *Build. Environ.* 94 (2015) 644–653.
- [13] B. Cheng, Z. Gou, F. Zhang, Q. Feng, Z. Huang, Thermal comfort in urban mountain parks in the hot summer and cold winter climate, *Sustain. Cities Soc.* 51 (2019) 101756.
- [14] T.-P. Lin, K.-T. Tsai, R.-L. Hwang, A. Matzarakis, Quantification of the effect of thermal indices and sky view factor on park attendance, *Landsc. Urban Plann.* 107 (2) (2012) 137–146.
- [15] Z. Peng, R. Bardhan, C. Ellard, K. Steemers, Urban climate walk: a stop-and-go assessment of the dynamic thermal sensation and perception in two waterfront districts in Rome, Italy, *Build. Environ.* Times 221 (2022) 109267.
- [16] Y. Tominaga, Y. Sato, S. Sadohara, CFD simulations of the effect of evaporative cooling from water bodies in a micro-scale urban environment: validation and application studies, *Sustain. Cities Soc.* 19 (2015) 259–270.
- [17] Y. Jiang, S. Jiang, T. Shi, Comparative study on the cooling effects of green space patterns in waterfront build-up blocks: an experience from Shanghai, *Int. J. Environ. Res. Publ. Health* 17 (22) (2020) 8684.
- [18] D. Shi, J. Song, J. Huang, C. Zhuang, R. Guo, Y. Gao, Synergistic cooling effects (SCEs) of urban green-blue spaces on local thermal environment: a case study in Chongqing, China, *Sustain. Cities Soc.* 55 (2020) 102065.
- [19] F. Fei, Y. Wang, W. Yao, W. Gao, L. Wang, Coupling mechanism of water and greenery on summer thermal environment of waterfront space in China's cold regions, *Build. Environ.* 214 (2022) 108912.
- [20] F. Fei, Y. Wang, X. Jia, Assessment of the mechanisms of summer thermal environment of waterfront space in China's cold regions, *Sustainability* 14 (5) (2022) 2512.
- [21] X.-c. Song, J. Liu, L. Yu, Pedestrian environment prediction with different types of on-shore building distribution, *J. Cent. S. Univ.* 23 (4) (2016) 955–968.
- [22] H. Xu, H. Chen, X. Zhou, Y. Wu, Y. Liu, Research on the relationship between urban morphology and air temperature based on mobile measurement: a case study in Wuhan, China, *Urban Clim.* 34 (2020) 100671.
- [23] G. Jang, S. Kim, J.S. Lee, Planning scenarios and microclimatic effects: the case of high-density riverside residential districts in Seoul, South Korea, *Build. Environ.* Times 223 (2022) 109517.
- [24] T. Xi, X. Zhang, W. Jin, W. Xu, Y. Wu, H. Qin, Primary exploration of leisure path design along songhua river by a small number of sample experiment, considering several multiple indexes, *Atmosphere* 13 (8) (2022) 1165.
- [25] W. Wang, H. Chen, L. Wang, S. Wang, Integrating multiple models into computational fluid dynamics for fine three-dimensional simulation of urban waterfront wind environments: a case study in Hangzhou, China, *Sustain. Cities Soc.* 85 (2022) 104088.
- [26] C. Waibel, T. Wortmann, R. Evins, J. Carmeliet, Building energy optimization: an extensive benchmark of global search algorithms, *Energ. Buildings* 187 (2019) 218–240.
- [27] Y. Wu, Q. Zhan, S.J. Quan, Improving local pedestrian-level wind environment based on probabilistic assessment using Gaussian process regression, *Build. Environ.* 205 (2021) 108172.
- [28] S. Wang, Y.K. Yi, N. Liu, Multi-objective optimization (MOO) for high-rise residential buildings' layout centered on daylight, visual, and outdoor thermal metrics in China, *Build. Environ.* Times 205 (2021) 108263.
- [29] L. Kabošová, A. Chronis, T. Galanos, S. Kmeť, D. Katunský, Shape optimization during design for improving outdoor wind comfort and solar radiation in cities, *Build. Environ.* 226 (2022) 109668.
- [30] X. Zheng, L. Chen, J. Yang, Simulation framework for early design guidance of urban streets to improve outdoor thermal comfort and building energy efficiency in summer, *Build. Environ.* 228 (2023) 109815.
- [31] Y. Zhang, J. Xu, Measurement and Analysis of Winter Microclimate of Waterfront Settlements in Severe Cold Region, IOP Conference Series: Materials Science and Engineering, IOP Publishing, 2019 012169.
- [32] W. Guo, T. Shen, L. Zhao, W. Deng, X. Pan, The effect of plants community on emperature and humidity of northern city in autumn, *Ecology and Environmental Sciences* 18 (4) (2009) 1422–1426.
- [33] R. Li, F. Zeng, Y. Zhao, Y. Wu, J. Niu, L.L. Wang, N. Gao, X. Shi, CFD simulations of the tree effect on the outdoor microclimate by coupling the canopy energy balance model, *Build. Environ.* (2023) 109995.
- [34] EPW Map. <https://www.ladybug.tools/epwmap/>.
- [35] Typical Weather Years. <https://designbuilder.co.uk/cahelp/Content/TypicalWeatherYears.htm>.
- [36] A. Ebrahimpour, New software for generation of typical meteorological year, *Weather* 1 (2011) 0BIntroduction.
- [37] A. Xu, Y. Dong, Y. Sun, H. Duan, R. Zhang, Thermal comfort performance prediction method using sports center layout images in several cold cities based on CNN, *Build. Environ.* 245 (2023) 110917.
- [38] R. Zhang, D. Liu, L. Shi, Thermal-comfort optimization design method for semi-outdoor stadium using machine learning, *Build. Environ.* 215 (2022) 108890.

- [39] N.H. Wong, Y. He, N.S. Nguyen, S.V. Raghavan, M. Martin, D.J.C. Hii, Z. Yu, J. Deng, An integrated multiscale urban microclimate model for the urban thermal environment, *Urban Clim.* 35 (2021) 100730.
- [40] R. Kadaverugu, V. Purohit, C. Matli, R. Biniwale, Improving accuracy in simulation of urban wind flows by dynamic downscaling WRF with OpenFOAM, *Urban Clim.* 38 (2021) 100912.
- [41] Y.K. Yi, N. Feng, Dynamic integration between building energy simulation (BES) and computational fluid dynamics (CFD) simulation for building exterior surface, *Build. Simulat.* 6 (3) (2013) 297–308.
- [42] F. Wu, X. Yang, Z. Shen, Regional and seasonal variations of outdoor thermal comfort in China from 1966 to 2016, *Sci. Total Environ.* 665 (2019) 1003–1016.
- [43] X. Song, J. Liu, Y. Zhao, Effect of design factors on the thermal environment in the waterfront area, *Procedia Eng.* 205 (2017) 2677–2682.
- [44] C. Sun, W. Lian, L. Liu, Q. Dong, Y. Han, The impact of street geometry on outdoor thermal comfort within three different urban forms in severe cold region of China, *Build. Environ.* 222 (2022) 109342.
- [45] S. Yilmaz, I. Sezen, M.A. Irmak, E.A. Külekçi, Analysis of outdoor thermal comfort and air pollution under the influence of urban morphology in cold-climate cities: Erzurum/Turkey, *Environ Sci Pollut R* 28 (2021) 64068–64083.
- [46] C.Y. Park, D.K. Lee, T. Asawa, A. Murakami, H.G. Kim, M.K. Lee, H.S. Lee, Influence of urban form on the cooling effect of a small urban river, *Landsc. Urban Plann.* 183 (2019) 26–35.
- [47] M. Xu, B. Hong, R. Jiang, L. An, T. Zhang, Outdoor thermal comfort of shaded spaces in an urban park in the cold region of China, *Build. Environ.* 155 (2019) 408–420.
- [48] P. Kastner, T. Dogan, Eddy3D: a toolkit for decoupled outdoor thermal comfort simulations in urban areas, *Build. Environ.* 212 (2022) 108639.
- [49] T.E. Morakinyo, K.K.-L. Lau, C. Ren, E. Ng, Performance of Hong Kong's common trees species for outdoor temperature regulation, thermal comfort and energy saving, *Build. Environ.* 137 (2018) 157–170.
- [50] A. Aboelata, Reducing outdoor air temperature, improving thermal comfort, and saving buildings' cooling energy demand in arid cities – cool paving utilization, *Sustain. Cities Soc.* 68 (2021) 102762.
- [51] K.B. Velt, H.A.M. Daanen, Thermal sensation and thermal comfort in changing environments, *J. Build. Eng.* 10 (2017) 42–46.
- [52] C. Chun, A. Kwok, T. Mitamura, N. Miwa, A. Tamura, Thermal diary: Connecting temperature history to indoor comfort, *Build. Environ.* 43 (5) (2008) 877–885.
- [53] C. Huang, G. Zhang, J. Yao, X. Wang, J.K. Calautit, C. Zhao, N. An, X. Peng, Accelerated environmental performance-driven urban design with generative adversarial network, *Build. Environ.* 224 (2022) 109575.